J Neurophysiol 123: 2297–2310, 2020.
First published May 6, 2020; doi:10.1152/jn.00105.2020.

RESEARCH ARTICLE | *Control of Movement*

Molecular characterization of frog vocal neurons using constellation pharmacology

Ryota T. Inagaki,[1] Shrinivasan Raghuraman,[1] Kevin Chase,[1] Theresa Steele,[2] Erik Zornik,[2] Baldomero Olivera,[1] and Ayako Yamaguchi[1]

[1]*School of Biological Sciences, University of Utah, Salt Lake City, Utah; and* [2]*Biology Department, Reed College, Portland, Oregon*

Submitted 2 March 2020; accepted in final form 4 May 2020

Inagaki RT, Raghuraman S, Chase K, Steele T, Zornik E, Olivera B, Yamaguchi A. Molecular characterization of frog vocal neurons using constellation pharmacology. *J Neurophysiol* 123: 2297–2310, 2020. First published May 6, 2020; doi:10.1152/jn.00105.2020.—Identification and characterization of neuronal cell classes in motor circuits are essential for understanding the neural basis of behavior. It is a challenging task, especially in a non-genetic-model organism, to identify cell-specific expression of functional macromolecules. Here, we performed constellation pharmacology, calcium imaging of dissociated neurons to pharmacologically identify functional receptors expressed by vocal neurons in adult male and female African clawed frogs, *Xenopus laevis*. Previously we identified a population of vocal neurons called fast trill neurons (FTNs) in the amphibian parabrachial nucleus (PB) that express *N*-methyl-D-aspartate (NMDA) receptors and GABA and/or glycine receptors. Using constellation pharmacology, we identified four cell classes of putative fast trill neurons (pFTNs, responsive to both NMDA and GABA/glycine applications). We discovered that some pFTNs responded to the application of substance P (SP), acetylcholine (ACh), or both. Electrophysiological recordings obtained from FTNs using an ex vivo preparation verified that SP and/or ACh depolarize FTNs. Bilateral injection of ACh, SP, or their antagonists into PBs showed that ACh receptors are not sufficient but necessary for vocal production, and SP receptors play a role in shaping the morphology of vocalizations. Additionally, we discovered that the PB of adult female *X. laevis* also contains all the subclasses of neurons at a similar frequency as in males, despite their sexually distinct vocalizations. These results reveal novel neuromodulators that regulate *X. laevis* vocal production and demonstrate the power of constellation pharmacology in identifying the neuronal subtypes marked by functional expression of cell-specific receptors in non-genetic-model organisms.

NEW & NOTEWORTHY Molecular profiles of neurons are critical for understanding the neuronal functions, but their identification is challenging especially in non-genetic-model organisms. Here, we characterized the functional expression of membrane macromolecules in vocal neurons of African clawed frogs, *Xenopus laevis*, using a technique called constellation pharmacology. We discovered that receptors for acetylcholine and/or substance P are expressed by some classes of vocal neurons, and their activation plays a role in the production of normal vocalizations.

constellation pharmacology; motor programs; parabrachial nucleus; premotor neurons; vocalizations

INTRODUCTION

A major goal of neuroscience is to understand the neural basis of behavior. Identifying types of neurons in a neural circuitry underlying behavior is critical in achieving this goal. Among a variety of cellular classification techniques (e.g., morphological, physiological, anatomical, immunohistochemical), the molecular genetics approach has become a powerful tool in illuminating functional roles played by different classes of neurons in recent years. Neuron types defined either by gene expression during development (Goulding 2009; Grillner and Jessell 2009) and/or in adulthood (Haque et al. 2018) can be used to classify and test the functionality of neurons. For example, spinal interneurons marked by the expression of Shox2 but not of Chx10 and glutamatergic spinal interneurons marked by Hb9 expression both play roles in locomotor rhythm generation in mice (Caldeira et al. 2017; Dougherty et al. 2013), and GABAergic Maf-expressing interneurons regulate the speed of locomotion in *Drosophila* (Babski et al. 2019). However, the use of molecular genetics to identify types of neurons is challenging in non-genetic-model organisms due to the limited availability of tools in these species. In this study, we applied a recently developed experimental approach called "constellation pharmacology" (Raghuraman et al. 2014) to characterize molecular profiles of neurons in the central vocal pathways of African clawed frogs, *Xenopus laevis*, a pseudotetraploid species with a long generation time that is challenging for genetic approach. In this technique, a series of target-selective pharmacological agents is applied to dissociated neurons while intracellular Ca^{2+} responses are monitored from ~1,000 neurons simultaneously; neurons can be classified into different classes based on unique combinations of functional receptors expressed by neurons.

Courtship vocalizations of a variety of vertebrate species are generated by central pattern generators (CPG) (Bass 2014; Konishi 2010; Sweeney and Kelley 2014), networks of neurons that generate rhythmic motor programs in the absence of rhythmic descending input or sensory feedback (Kiehn 2006; Marder and Bucher 2001). In this study, we identified the molecular profiles of neurons in the vocal CPG of *X. laevis* that offers advantages for the analyses of the neural basis of behavior due to its experimental amenability. Fictive vocalizations (i.e., rhythmic motor activity produced by an isolated brain preparation ex vivo that are facsimiles of neuronal

Correspondence: A. Yamaguchi (a.yamaguchi@utah.edu).

activity generated during vocal production in vivo) can be readily and repeatedly elicited from the isolated brains of adult *X. laevis* in response to the application of serotonin (5-HT) (Rhodes et al. 2007). Using this preparation, we have previously identified a population of premotor neurons called fast trill neurons (FTNs) in the amphibian parabrachial nucleus (PB, previously labeled as the dorsal tegmental area of medulla, DTAM) that code for the duration and the rate of the male advertisement calls by driving laryngeal motor neurons (Zornik and Yamaguchi 2012). Based on whole-cell patch-clamp recordings obtained from FTNs, we identified that the neurons express *N*-methyl-D-aspartate (NMDA) receptors (NMDAR) and GABA and/or glycine (Gly) receptors (Lawton et al. 2017; Zornik and Yamaguchi 2012).

Using constellation pharmacology, we identified four subclasses of putative FTNs (pFTNs) based on their responsiveness to NMDA and GABA and/or Gly. We discovered that some of the pFTNs responded to acetylcholine (ACh) and/or substance P (SP). Although the involvement of these neuromodulators in vocal motor programs was previously unknown, electrophysiological recordings using the ex vivo preparation confirmed that FTNs indeed depolarize in response to the application of ACh and/or SP. Furthermore, bilateral injections of antagonists and agonists for ACh and SP into PBs revealed that ACh is necessary but not sufficient for the vocal production, and SP plays a role in shaping the morphology of normal vocal motor programs. Furthermore, all subclasses of neurons identified in adult male PB are also present at a similar frequency in adult female PB even though vocalizations are sexually distinct in *X. laevis* (Kelley 1986). This study highlights the synergistic power of the constellation pharmacology and electrophysiological technique in identifying molecular profiles of neurons important for behavior in non-genetic-model organisms.

MATERIALS AND METHODS

Animals. Adult *Xenopus laevis* frogs (male, $n = 24$, 4.5~7.2 cm, 9.6~37.0 g; female, $n = 5$, 4.4~5.4 cm, 11.0~18.2 g) were obtained from NASCO. Sexually mature male *X. laevis* produce advertisement calls to attract females when they are sexually receptive, and adult females produce release calls to repel males when they are not sexually receptive. We ensured all the males and females used in the present study to be in the appropriate physiological state to produce advertisement or release calls, respectively. For males used in ex vivo whole-cell patch-clamp experiments and whole-brain fictive recording experiments, only the brains that generated fictive advertisement calls in response to the application of 5-HT were used. For the males used for the constellation pharmacology experiments, human chorionic gonadotropin was injected (hCG; Sigma-Aldrich) subcutaneously to bring them into sexual receptivity and vocalizations were recorded using hydrophones 1 to 7 days before the experiments; only the males that generated advertisement calls were used for the experiments. Females housed with other females in captivity remain sexually unreceptive. Therefore, for the constellation pharmacology experiments females that were not pretreated with hCG were used. All the procedures were approved by the Institutional Animal Care and Use Committee at the University of Utah.

Primary culture of neurons. Animals were anesthetized with 1.3% tricaine methanesulfonate (MS222; 300–500 μl; Sigma-Aldrich). Immediately after decapitation, the isolated skull was placed on a 100-mm Petri dish filled with ice-cold frog saline (in mM: 103 NaCl, 13 $NaHCO_3$, 2 $CaCl_2$, 2 KCl, 0.5 $MgCl_2$, HEPES, and 11 dextrose, pH 7.8) oxygenated with 99% O_2 and 1% CO_2. A brain was dissected out from the skull, and all meninges were removed from the brain for slice preparation. The isolated brain was attached to a vibratome chamber filled with ice-cold saline and sliced transversely (250~300 μm in thickness), a protocol previously established for electrophysiological experiments (Yamaguchi et al. 2003). Under a stereomicroscope, PBs were visualized and were cut out from the brain slice using a scalpel and transferred into a centrifuge tube with 1 ml of frog saline. Neurons were dissociated first by placing the tissue in 2.5% Trypsin for 10 min, and washed three times with 5 ml of Frog Neuronal Culturing Medium (FNCM; 49% Frog Culturing Ringer in mM: 115 NaCl, 1 Na-pyruvate, 2 $CaCl_2$, 2 KCl, 0.5 $MgCl_2$, 10 HEPES, and 11 dextrose, 49% L-15 medium, 1% fetal bovine serum, 1% penicillin-streptomycin, pH 7.8). The tissue was then triturated with Pasteur pipette until the whole tissue was dissociated and the solution became translucent, centrifuged at 1,100 rpm (136 G) for 10 min, and concentrated by removing the supernatant. A sterilized silicon ring (10-mm silicon ring with a 3-mm-diameter hole in the center) was placed on the bottom of polylysine-coated culture wells (Corning). Twenty-five to 30 μl of the dissociated cell suspension was applied on the center of silicon rings, 1 ml of FNCM was added to the culturing chamber in an hour, and the neurons were incubated overnight at 20 to 22°C. Although dissociated cells consist mostly of somata and short processes, functional receptors and ion channels specific for each cell types are known to be expressed by somata (Curtice et al. 2016; Imperial et al. 2014; Raghuraman et al. 2014; Teichert et al. 2012, 2014).

Calcium imaging. Dissociated neurons were loaded with a FURA-2 dye (2.5 μM, 700 μl, 380 nm excitation/510 nm emission) for at least 1 h before the start of an imaging experiment. The FURA-2-loaded cells were excited alternately with 340 nm and 380 nm light every 2 s, and a video image was obtained. The ratio of fluorescent intensities measured at 510 nm emission provides a relative measure of cytosolic calcium concentration ($[Ca^{2+}]_i$) (Iredale and Dickenson 1995). The 340/380 nm ratio of fluorescence intensity was calculated over time to trace the relative shift of $[Ca^{2+}]_i$ for each cell. Cells exhibit variable capabilities to absorb FURA-2 and, thus, load unevenly. This resulted in heterogeneous baseline fluorescence among cells. The use of ratiometric imaging allowed us to normalize the uneven loading of the cells, and obtain measurements of the changes in the $[Ca^{2+}]_i$ within each cell in response to ligand applications. We obtained recordings from 1~3 wells per animal, 574 to 1,378 cells imaged per well at $\times 10$ objective/magnification. Cells are defined as regions of interest (ROIs) using a bright-field image. Traces are ratiometric values for each ROI in the series of images taken at 2-s intervals over the time frame of the experiment.

The concentration and abbreviation of pharmacological agents used for this study are summarized in Table 1. For all experiments, 700 μl of the pharmacological agents were applied every 7 min. Each ligand was applied for 10 s followed by three washes to clear the pharmacological agent from the wells. The application of ligands was manual and the solutions were aspirated using a vacuum pump controlled by a foot pedal.

All neurons that responded to GABA with glycine, and NMDA with D-serine were considered to be putative FTNs (pFTNs) based on our previous electrophysiological recordings obtained from the neurons using ex vivo preparation; FTNs showed inhibitory postsynaptic potentials (IPSPs) during fictive vocal productions, and when pharmacologically isolated from all chemical synapses by applying TTX, the membrane potentials of FTNs oscillated in response to the application of NMDA (Zornik and Yamaguchi 2012). Since IPSPs exhibited by FTNs could be mediated by GABA and/or glycine, we used a combination of both to identify the putative FTNs.

Whole-cell patch-clamp electrophysiological recordings. Whole-cell patch-clamp recordings were obtained from neurons in PB using a whole-brain, ex vivo preparation, as previously described (Zornik and Yamaguchi 2012). Briefly, patch-clamp electrodes (6–10 MΩ) made from thick-walled borosilicate capillary tubes (1.5-mm outer

Table 1. *Abbreviation and working concentration of pharmacological agents*

Abbreviation	Pharmacology Agent	Working Concentration	Target Receptor
NMDA	*N*-methyl-D-aspartate	200 μM	NMDA-receptor
SP	Substance P	1 μM	Neurokinin-1-receptor
ACh	Acetylcholine	1 mM	Acetylcholine-receptor
ATP	Adenosine 5′ triphosphate	20 μM	Purinergic-receptor
5-HT	Serotonin	25 μM	5-HT-receptor
GABA	γ-Aminobutyric acid	1 mM	GABAergic-receptor
Gly	Glycine	1 mM	Glycinergic-receptor
D-Ser	D-Serine	20 μM	NMDA-receptor
H	Histamine	50 μM	Histamine-receptor
Br	Bradykinin	10 μM	Bradykinin-receptor

diameter; 0.86-mm inner diameter), were used to blind search for FTN by advancing the pipette vertically into PB using a motorized micromanipulator (MC1000e; Siskiyou). The cells were determined to be FTNs based on their membrane potential activity (Fig. 5*A*) synchronized with 5-HT-induced fictive fast trills. Intracellular solution contained the following (in mM): 115 KCl, 2 $MgCl_2$, 2 EGTA, 10 HEPES, 2 MgATP, and 0.2 NaGTP, pH 7.4. Once FTN is identified, the neuron was pharmacologically isolated from action potential-mediated synaptic inputs by applying 1 μM of TTX to the whole brain. ACh (1 mM final concentration) or SP (1 μM final concentration) was bath applied for 10 min to determine whether the resting membrane potential of the neuron (averaged over 30 s) change before, during, and after the application.

Ex vivo, isolated brain preparation, PB injections, and fictive vocal recordings. Fictive vocalizations were elicited from the isolated brains of sexually mature adult males. Brains were isolated as described above (*Primary culture of neurons* section) and gradually returned to room temperature (22°C) over the next hour, and then transferred to a recording chamber superfused with oxygenated saline at 100 ml/h.

Laryngeal nerve activity was recorded bilaterally using a suction electrode placed over cranial nerve (N.) IX-X. Local field potential (LFP) recordings from PBs were obtained bilaterally using a 1 MΩ tungsten electrode (FHC, Bowdoin, ME) to confirm the location of PBs before injection. During the fast trill portion of the fictive advertisement call, PBs shows a stereotyped baseline wave superimposed with ~60-Hz phasic activity (Zornik and Yamaguchi 2012). Prior to the start of the experiment, 5-HT (Sigma, 30 μM, final concentration) was bath applied to elicit fictive advertisement calls. To examine whether substance P (SP) and acetylcholine (ACh) are sufficient to elicit fictive vocalizations, 350 nl of 1 μM SP or ACh solution including Texas Red dissolved in saline was injected into both PBs using Nanoject (Drummond Scientific) at a rate of 10 nl/s. It took a total of ~90 s to complete the bilateral injection: 35 s to inject into each PB, and up to 20 s to switch the injection pipette from one PB to the other. Nerve recordings were obtained during the injection as well as for 5 min following the injection. To determine whether ACh and SP are necessary for the fictive vocal production, a combination of atropine (1 mM) and tubocurarine (1 mM, both dissolved in saline, including Texas Red) or aprepitant (a neurokinin-1 receptor antagonist, 0.4 mM dissolved in 10% DMSO in frog saline, including Texas Red) were injected bilaterally into PBs (350 nl each) using the methods described above, followed by the bath application of 5-HT within 10 s of the completion of the injection. Five minutes after the injection and/or application of 5-HT, superfusion was reinstated at the maximum rate (~10 ml/min) for 5 min to wash out the 5-HT, then at a slower rate (~125 ml/h) for 1–4 h. To test the effects of the vehicles on the PBs, the experiments were repeated using injections of vehicles alone (350 nl of saline or 10% DMSO in saline at 10 nl/s on each side) followed by the bath application of 5-HT. Except for ACh injection experiment (see RESULTS, Fig. 6*B*), only brains that showed vocal recovery following the experimental treatment were used for the analyses.

Nerve and LFP signals were amplified using differential amplifiers (models 1700 and 1800, respectively; A-M Systems, Carlsborg, WA), and band-pass filtered (10 Hz to 5 kHz and 0.1–5 kHz, respectively). All signals were digitized at 10 kHz (Digidata 1440A; Molecular Devices, Sunnyvale, CA), and recorded on a PC using Clampex software (Molecular Devices).

Histology. Brains injected with pharmacological agents were fixed with 4% paraformaldehyde overnight at 4°C, placed into 30% sucrose solution for 24 h, and horizontally sectioned into 30-μm thickness using a freezing sliding microtome. Sections were counterstained using NeuroTrace 500/525 (Thermofisher Scientific). Injection sites were photographed and analyzed under an Olympus BX41 microscope with a digital camera (Retiga 2000R, QImaging, Surrey, Canada).

Constellation pharmacology data analyses. For imaging experiments, ratiometric values are indicators of internal calcium levels. The time-course of the ratio was analyzed using a set of functions written in R (Team 2013). The maldiquant package (Gibb and Strimmer 2012) was used to correct baselines, smooth, and detect peaks. All traces were baseline corrected using the estimateBaseline function with the "SNIP" method and smoothed using the smoothIntensity function with the "SavitzkyGolay" method and a half WindowSize of 3. Peaks were detected using the detectPeaks function with the "MAD" method, a halfWindowSize of 30 and a SNR.lim setting of 4. All ROIs were scored as yes/no response to each input based on the presence of a peak in the response window of 30 s following the application of pharmacological agents. Thresholds were established to define possible peaks in the response window. We used a signal-to-noise ratio threshold of 4 with at least a value above the baseline threshold of 0.05 to control for false-positive in regions of very low variance in recordings. These threshold values give a false-positive rate <0.001 (e.g., peaks during times of no input). Traces with obvious abnormal response patterns were removed from the analysis.

Fictive vocalizations data analyses. The bath application of 5-HT to the brains bilaterally injected with aprepitant into the parabrachial nucleus elicited fictive advertisement calls with abnormal morphology in terms of the amplitude and the frequency of the compound action potentials (CAPs). To quantitatively compare the morphology of the fictive advertisement calls produced in the presence and absence of aprepitant, we measured the peak amplitude and the instantaneous frequency (i.e., reciprocal of the inter-CAP interval) of the CAPs generated before, during, and after (vehicle alone) the injection of aprepitant and plotted it against the order of the CAPs. Three to 10 calls were sampled from each experimental condition of each animal, and cross-correlation coefficients of the peak amplitude and instantaneous frequency profile of the calls were calculated from all pair-wise combinations [i.e., $n*(n-1)/2$ for each condition, where n stands for the total number of songs sampled for each condition from each animal]. The average and the standard deviation of cross-correlation coefficients were calculated for each experimental condition in each animal. High coefficients close to 1 indicate more stereotyped call morphology.

Data availability. The data that support the findings of this study are available from the corresponding author upon reasonable request.

RESULTS

Monitoring intracellular calcium in live parabrachial neurons. Although culturing neurons of adult vertebrate animals has been difficult (Eide and McMurray 2005), we were able to obtain healthy dissociated cell cultures of optimal density (885 ± 222 cells per culturing chamber, mean ± standard deviation, $n = 17$ chambers) from adult parabrachial (PB) nucleus as shown in Fig. 1*A*. The optimization of dissociation protocol, attachment substrates, and culture media, are described in detail in MATERIALS AND METHODS. Figure 1, *B* and *C* shows fluorescence images from the same field of view as shown in the bright-field image in Fig. 1*A*. Pseudocolored ratiometric images of $[Ca^{2+}]_i$ are acquired at rest (Fig. 1*B*) and are monitored continuously for the duration of the experiment. Figure 1*C* shows the image acquired when the high extracellular concentration of KCl (30 mM, high $[K^+]_o$) stimulus elicited an increase in $[Ca^{2+}]_i$ in a subset of cells. Because the expression of voltage-gated Ca^{2+} channels is seen in neurons but not in glial cells (Carmignoto et al. 1998), increased $[Ca^{2+}]_i$ in response to high $[K^+]_o$ was taken as a proxy for neurons. Among all dissociated cells, 85.0 ± 6.7% (mean ± standard deviation, $n = 8$) of cells were classified as neurons; the proportion of neurons among all dissociated cells was consistent across individuals, as evident in the small value of the standard deviation.

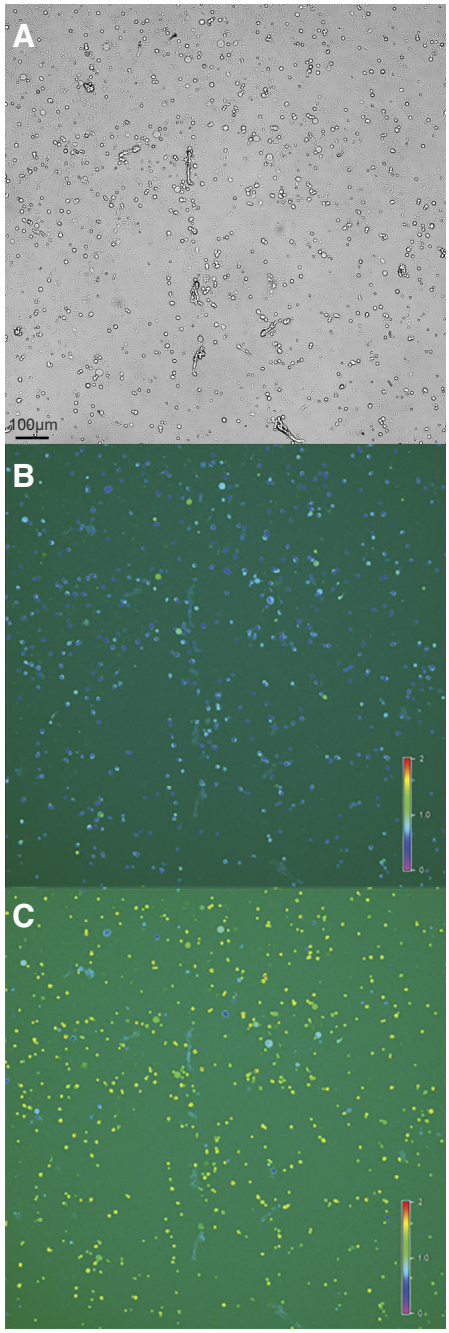

Fig. 1. Images of dissociated cells obtained from parabrachial nucleus (PB) of male *Xenopus laevis*. *A*: bright-field image of dissociated cells from PB. *B*: pseudocolored ratiometric calcium image acquired at resting condition. Note that many cells are blue in color indicating low cytoplasmic $[Ca^{2+}]$. *C*: pseudocolored ratiometric calcium image during application of 30 mM KCl. Note that many cells are in green to yellow color, indicating higher cytoplasmic $[Ca^{2+}]$.

Classification of PB neurons using constellation pharmacology. Once the neurons were distinguished from glial cells among all dissociated PB cells with high $[K^+]_o$, we serially applied a panel of pharmacological agents and monitored $[Ca^{2+}]_i$ responses from ~500 to 1,000 dissociated neurons simultaneously. Activation of receptors that depolarize the membrane potentials, which in turn increase the conductance of voltage-gated Ca^{2+} channels, were observed as increases in $[Ca^{2+}]_i$. In contrast, activation of GABA and/or Gly receptors that hyperpolarize the membrane potentials were deduced indirectly using the following method. High $[K^+]_o$ was applied three times with 7-min intervals and Ca^{2+} signals obtained from these three applications were compared (Fig. 2). Between the first and the second high $[K^+]_o$ exposure, the cells were incubated with the combination of GABA and Gly. If the cells express GABA and/or Gly receptors, the second high $[K^+]_o$ results in either reduced or no Ca^{2+} signals due to the increased influx of I_{Cl}^- that counteracts the membrane depolarization. The recovery of the calcium signal on the 3rd high $[K^+]_o$ is used as a control to verify that the reduction/elimination of Ca^{2+} signals during the 2nd high $[K^+]_o$ was due to the GABA and Gly application and not due to general deterioration of the health or desensitization of the cells (Fig. 2).

In addition to two ligand groups that are known or suspected to elicit responses from the FTNs (NMDA with D-serine, GABA with glycine), we tested whether 5-HT, a neurotransmitter that initiates fictive vocalizations, modulates the excitability of the FTNs. Furthermore, we selected five additional ligands (histamine, bradykinin, acetylcholine, substance P, and ATP) that are known to be involved in regulating respiratory rhythms in the brainstem (Doi and Ramirez 2008; Funk 2013; Raghuraman et al. 2014; Ramirez et al. 2018; Shao and Feldman 2009) to classify FTNs. The vocal neural circuitry is considered to have evolutionarily originated from the respiratory neural circuitry (Bass and Baker 1997), and thus we hypothesized that there is a significant overlap in receptors expressed by the respiratory and vocal neural circuitry. Histamine and bradykinin, however, elicited responses from very few dissociated *X. laevis* PB neurons (2.5 ± 0.05% and 2.5 ± 0.70% of all neurons, mean ± standard deviation, respectively, $n = 2$). Thus, we focused on the remaining 6 ligand groups to

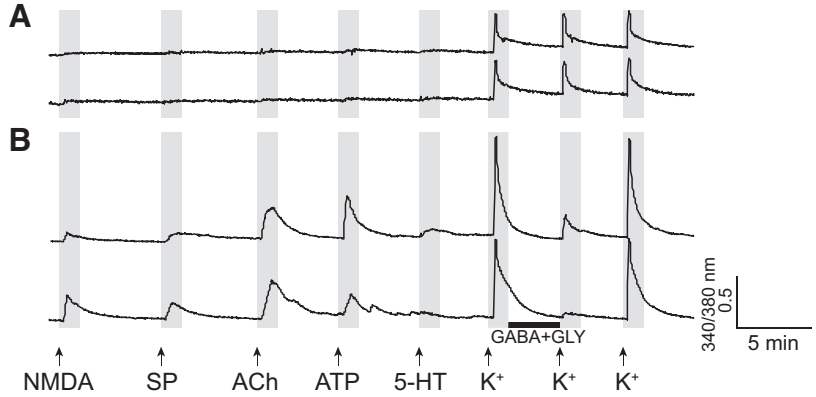

Fig. 2. Example calcium imaging traces from two parabrachial neurons. The *x*-axis and *y*-axis indicate time and a relative measurement of cytoplasmic $[Ca^{2+}]$, respectively. Arrows indicate the time at which pharmacological agents were applied, and the black horizontal bar indicates the time during which cells were incubated with GABA and glycine (Gly). *A*: two traces that exemplify neurons that show consistent response to a high concentration of $[K^+]_o$ but do not respond to any other ligands applied. These neurons belong to class B-III (Table 2). *B*: two traces that exemplify neurons that respond to the application of *N*-methyl-D-aspartate (NMDA), substance P (SP), ACh, ATP, and GABA with glycine, but not to the application of 5-HT. The neurons belong to pFTN-IV (Table 2). In *A*, the peak $[Ca^{2+}]_i$ transient amplitude in response to the second $[K^+]_o$ (preceded by incubation with GABA and glycine) is the same as those in response to the first and third $[K^+]_o$, whereas, in *B*, the second application of $[K^+]_o$ elicits reduced responses compared with the first and third $[K^+]_o$ applications. These response profiles are taken as evidence for the lack (*A*) or presence (*B*) of the functional expression of the receptors for GABA and/or glycine, respectively.

classify FTNs (Table 1, four of the ligands, NMDA with D-serine and GABA with Gly, were coapplied as pairs). It should be noted that, although the combination of GABA and Gly were applied to dissociated cells in most experiments, we discovered in a separate experiment ($n = 3$) that PB cells sensitive to a cocktail of GABA and Gly responded to GABA alone (34 ± 15%), to Gly alone (1 ± 1%), or to both (65 ± 14%), indicating that ~99% of PB neurons that show inhibitory responses express GABA receptors, two-third of which additionally express Gly receptors.

Representative calcium imaging traces obtained from two PB neurons are shown in Fig. 2. Figure 2*A* shows a Ca^{2+} profile of two neurons that responded to high $[K^+]_o$, but not to any other pharmacological agents. Figure 2*B* exemplifies a type of neuron that responded to the NMDA with D-serine, SP, ACh, ATP, and GABA with Gly (the neuron on the *top trace* responded to 5-HT in addition). These traces reveal that the two groups of neurons have a distinct combination (constellation) of membrane receptors and thus can be classified as two distinct types.

To classify cell types contained in the PB of male *X. laevis*, we first used both cell size and Ca^{2+} profile in response to a high $[K^+]_o$, and ATP to subdivide neurons into two major classes, A and B (see the following two paragraphs). The sizes of the dissociated PB neurons were heterogeneous, consistent with our previous observations in brain slice and fixed brain preparations (A. Yamaguchi, unpublished data). Neuron classes A and B were further divided into subclasses based on their response profile to a series of agonists (Table 2).

Class A cells (Table 2) are defined as neurons with a surface area $>100\ \mu m^2$ (Table 2, Fig. 3*A*, *left*) with the following response property; they exhibit transient $[Ca^{2+}]_i$ increase in response to ATP with the peak amplitude larger than those in response to high $[K^+]_o$ (Fig. 3*B*). Class A cells constitute 17 ± 3% ($n = 8$) of all dissociated cells obtained from male *X. laevis*. Although all class A cells responded to ATP, they responded differently to other agonists, and can be divided further into five subclasses based on their response profile (Table 2). Although some class A cells showed responses to NMDA with D-serine or to GABA with Gly application (Table 2), none of the cells responded to both. Thus, class A cells were ruled out from being putative FTNs.

Class B cells are defined as neurons with a surface area $<150\ \mu m^2$ (Fig. 3*A*) with a transient $[Ca^{2+}]_i$ increase with a peak amplitude in response to a repeated application of high $[K^+]_o$ consistently higher than those in response to any other ligands (Fig. 3*C*). Class B cells constitute the majority of dissociated PB cells in males (68 ± 4%, $n = 8$). The class B cells can be further divided into seven subclasses (Table 2), four of which responded to both NMDA with D-serine and GABA with Gly, a response profile consistent with FTNs. Thus, we considered these subclasses of neurons as putative FTNs (pFTNs), and investigated them further. Figure 4 shows the examples of calcium imaging traces obtained from all four subclasses of pFTNs (pFTNs I through IV) in response to the application of an array of ligands. Although 5-HT is potent in eliciting fictive vocalizations, the proportion of pFTNs that responded to 5-HT was relatively low (9–20%, Table 2). In addition, responses to ATP was also low and variable (14–42%, Table 2). Thus, the responsiveness to these two ligands was not used to categorize subclasses of pFTNs (Table 2). Four subclasses of pFTNs exhibited the following response profiles. The most common subclass, pFTN-I (30 ± 3% of all dissociated neurons, $n = 8$), did not respond to substance P (SP) nor acetylcholine (ACh, Fig. 4*A*, Table 2). The second most frequent subclass, pFTN-II (11 ± 1%, $n = 8$) responded to SP (Fig. 4*B*, Table 2). The third most common subclass, pFTN-III (5 ± 1%, $n = 8$), responded to ACh (Fig. 4*C*, Table 2). The least common subclass, pFTN IV (3 ± 1%, $n = 8$), responded to both SP and ACh (Fig. 4*D*, Table 2).

Validating in vitro findings in intact circuits. Among four subclasses of pFTNs, three showed responsiveness to ACh, SP, or both. To determine whether FTNs are indeed sensitive to ACh and/or substance P, we carried out whole-cell patch-clamp recordings from FTNs in an ex vivo, whole-brain preparation. After FTNs were functionally identified based on the firing patterns during fictive advertisement calls elicited in response to the bath application of 5-HT (Fig. 5*A*), the neurons

Table 2. *The classification of cell types obtained from the parabrachial nucleus of male Xenopus laevis*

Cell Types	Classification Criteria	Total No. of Cells	% Cells/Animal (mean + SE)	% Response to Pharmacological Agents (mean + SE)					
				NMDA	SP	ACh	ATP	GABA	5-HT
Neurons	+[K^+]	11,074	85+7	69+0.4	32+0.4	29+0.4	38+0.5	58+0.5	28+0.4
Class A K^+ amp (0.18+0.003)* Cell area (214+1.7 μm^2)*	K^+amp<ATP amp >100 μm^2	1,902	17+3	18+0.9	49+1.1	89+0.7	100	8+0.6	87+0.8
A-I	+[SP,ATP,ACh,5-HT]	879	9+2	20+1	100	100	100	6+1	100
A-II	+[SP,ATP] −[ACh,5-HT]	59	1+0	59+6	100	0	100	29+6	0
A-III	+[ATP,ACh,5-HT] −[SP]	636	6+1	12+1	0	100	100	6+1	100
A-IV	+[ATP,5-HT] −[SP,ACh]	142	2+0	20+3	0	0	100	15+3	100
A-V	+[ATP] −[SP,ACh,5-HT]	186	2+1	10+2	0	100	100	10+2	0
Class B K^+ amp (0.61+0.002)* Cell area (74+0.28 μm^2)*	<150 μm^2	9,172	68+4	80+0.4	28+0.5	17+0.4	25+0.5	68+0.5	15+0.4
pFTN-I	+[NMDA,GABA] −[SP,ACh]	3,245	30+3	100	0	0	14+1	100	9+1
pFTN-II	+[NMDA,GABA,SP] −[ACh]	1,271	11+1	100	100	0	36+1	100	16+2
pFTN-III	+[NMDA,GABA,ACh] −[SP]	550	5+1	100	0	100	19+2	100	15+2
pFTN-IV	+[NMDA,GABA,SP,ACh]	400	3+1	100	100	100	42+2	100	20+1
B-I	+[NMDA] −[GABA]	1,882	14+4	100	29+1	19+1	26+1	0	17+1
B-II	+[GABA] −[NMDA]	783	7+2	0	16+1	6+1	20+1	100	15+1
B-III	−[NMDA,GABA]	1,041	10+2	0	23+1	16+1	51+2	0	32+1
Nonneuronal cells	−[K^+]	2,011	15+3	33+5	32+3	42+4	40+3	NA	22+3

"Classification criteria" describes characteristics used to define classes and subclasses of cells. +[ ] and −[ ] indicates the presence and absence of Ca^{2+} responses to the pharmacological agents contained in the brackets, respectively. "Total no. of cells" indicates all the cells that were categorized into classes of neurons across 8 animals. "% cells/animal" indicates mean ± standard error (SE) of the proportion of cells that were categorized into each class within each animal. "% responses to pharmacological agents" show mean *U* SE of the proportion of neurons that responded to each ligand within each class and subclass. The threshold criteria to define the presence and absence of responses are described in MATERIALS AND METHODS. *Asterisks in the first column indicate mean ± SE of the peak Ca amplitude (amp) in response to a high K^+ application and the surface area for Class A and Class B neurons. FTN, fast trill neurons; NMDA, *N*-methyl-D-aspartate, SP, substance P.

were pharmacologically isolated from action potential-mediated synaptic inputs by applying 1 μM TTX to the whole brain, and the changes in the membrane potential were measured in response to the bath application of ACh (1 mM) or SP (1 μM) in a current-clamp mode (Fig. 5*B*). The results showed that three of four FTNs depolarized in response to both ACh and SP, and the remaining one neuron depolarized only in response to ACh (Fig. 5*C*). All of the neurons hyperpolarized after the ligands are washed out from the bath (Fig. 5, *B* and *C*). The results confirmed that FTNs in intact circuits indeed express ACh and NK-1 receptors and are likely to include pFTN III and IV.

Role of substance P and acetylcholine in fictive vocalizations. If FTNs depolarize in response to SP and ACh, what are the functions of these neurotransmitters in the vocal pathways of male *X. laevis*? We first examined whether SP and ACh are sufficient to elicit fictive advertisement calls by injecting SP (1 μM) or ACh (1 mM) bilaterally into PBs (350 nl into each side) using an ex vivo whole-brain preparation while recordings were obtained from the laryngeal motor nerves ($n = 4$ for SP, $n = 8$ for ACh). By including Texas Red in the injection solution, the targeting of PBs was confirmed histologically post hoc (Fig. 6*A*). The results showed that the bilateral injection of ACh into PBs failed to elicit fictive advertisement calls in all the brains, although tonic activity was recorded from the laryngeal motor nerves during the injection in some brains (Fig. 6*C*, *middle trace*). After 1 to 4 h of wash, none of the ACh-injected brains generated fictive advertisement calls in response to the bath application of 5-HT (Fig. 6*C*, *right trace*). In contrast, brains ($n = 6$) that received bilateral saline (vehicle) injection of the same volume (350 nl) into PBs generated fictive calls in response to the bath application of 5-HT after 1 to 2 h of wash (data not shown). The results indicate that the lack of vocal recovery in ACh-injected brains are due not to any mechanical damage incurred to the PBs, but to a long-lasting inhibitory effect of ACh on the central vocal pathways. In contrast, bilateral injections of SP into PBs ($n = 4$) resulted in the variable outcome; one brain generated fast trills (Fig. 6*D1*), another brain produced slow trills (Fig. 6*D2*), and the two remaining brains generated no fictive vocalizations even though the bath application of 5-HT after 1 to 2 h of wash elicited fictive vocalizations (Fig. 6*D3*). The bath application of ACh (1 mM) and SP (1 μM) mirrors the PB injection results; the bath application of ACh ($n = 3$) did not elicit fictive vocalizations from any of the isolated brains, whereas the bath application of SP ($n = 7$) elicited fictive advertisement call from one brain, fictive slow trills from three brains, and no calls from the remaining three brains (data not shown). The brains that did not sing in response to the bath application of ACh and SP generated fictive vocalizations in response to

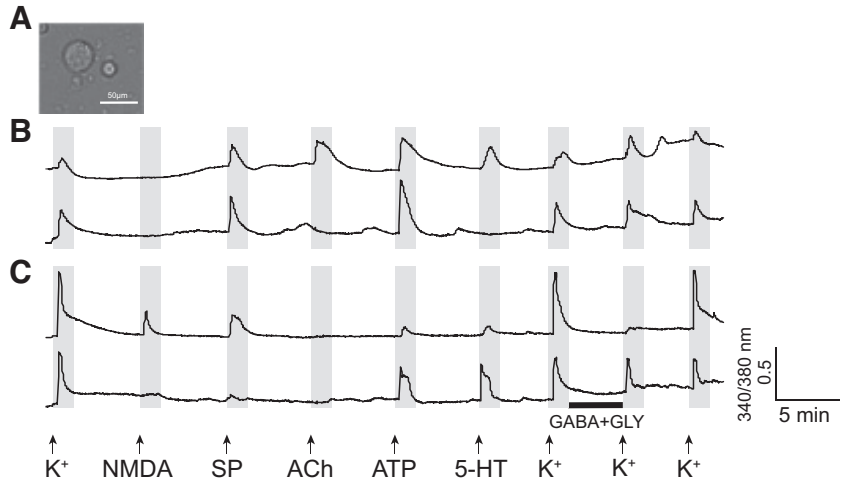

Fig. 3. Characteristics of class A and class B neurons. *A*: a photomicrograph of representative class A (*left*, larger) and B (*right*, smaller) neurons. *B*: two example calcium imaging traces of class A neurons. The *x*- and *y*-axes indicate the time and a relative measurement of cytoplasmic $[Ca^{2+}]$, respectively. Arrows indicate the time at which pharmacological agents were applied, and the black horizontal bar indicates the time during which cells were incubated with GABA and glycine (Gly). Note that the peak amplitude of $[Ca^{2+}]$ transients in response to a high concentration of $[K^+]_o$ is smaller compared with the peak amplitude in response to ATP, and this is one of the criteria we used to define class A neurons. The *top* and *bottom traces* are examples of class A-I and class A-II, respectively (Table 2). Many class A neurons show intrinsic $[Ca^{2+}]$ oscillation in the absence of any ligands, as evidenced in these traces, for reasons that are not clear. *C*: two example calcium imaging traces of class B neurons. The *top* and *bottom traces* are examples of pFTN-II and B-III neurons, respectively. Note that the peak amplitude of $[Ca^{2+}]$ transients in response to a repeated application of a high concentration of K^+ is consistently higher than those in response to other ligands.

5-HT 1 to 2 h after the wash, indicating that these brains were capable of generating fictive vocalizations. Given that the concentrations of the bath applied ACh and SP are the same as those that depolarize the membrane potential in the previous whole-cell patch-clamp recordings using the same ex vivo preparation (Fig. 5*C*), the results suggest that the depolarization of FTNs by ACh is not sufficient to elicit fictive vocalizations, and the excitation of FTNs by SP can activate the vocal CPG in some brains but its potency is lower than that of 5-HT.

Next, we examined whether these two neurotransmitters are necessary for the activation of the vocal pathways. To this end, a combination of atropine (a muscarinic ACh receptor antagonist, 1 mM) and tubocurarine (a nicotinic ACh receptor antagonist, 1 mM) or aprepitant (a neurokinin-1 receptor antagonist, 0.4 mM) were injected bilaterally (350 nl each) into PBs just before 5-HT was applied to the bath ($n = 5$ for atropine/tubocurarine, $n = 3$ for aprepitant). When 5-HT was applied to the brain that received bilateral injections of atropine/tubocurarine, none of the brains generated fictive adver-

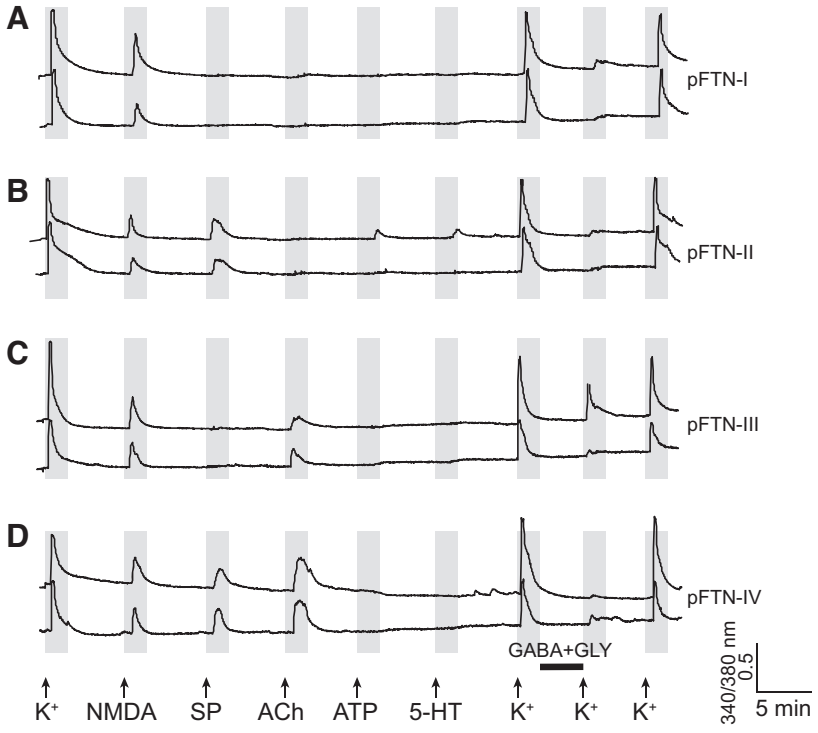

Fig. 4. Example calcium imaging traces of putative fast trill neurons (pFTN) I through IV. The *x*- and *y*-axes indicate the time and a relative measurement of cytoplasmic $[Ca^{2+}]$, respectively. Arrows indicate the time at which pharmacological agents were applied, and the black horizontal bar indicates the time during which cells were incubated with GABA and glycine (Gly). *A*: two example calcium imaging traces from pFTN-I. These neurons respond to *N*-methyl-D-aspartate (NMDA) and GABA with glycine application, but not to ACh or substance P (SP). *B*: two example calcium imaging traces of pFTN-II. These neurons respond to NMDA, GABA with glycine, and SP. *C*: two example calcium imaging traces of pFTN-III. These neurons respond to NMDA, GABA with glycine, and ACh application. *D*: two example of calcium imaging traces of pFTN-IV. These neurons respond to NMDA, GABA with glycine, SP, and ACh application.

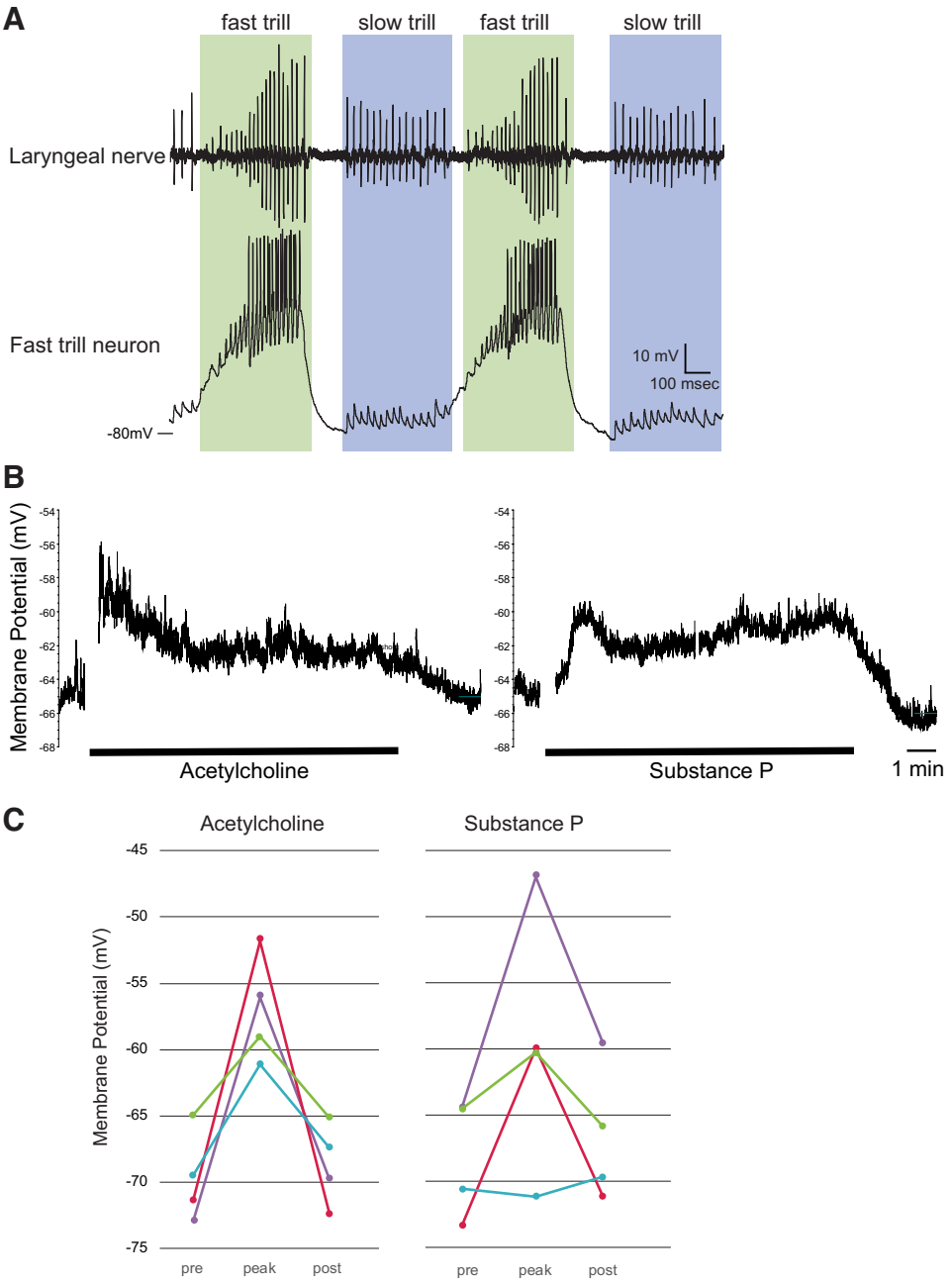

Fig. 5. Responses of fast trill neurons (FTNs) to acetylcholine (ACh) and substance P (SP). *A*, *top trace*: recordings obtained from the laryngeal nerve of isolated brain preparation. *Bottom trace*: membrane potential recorded from the FTN during fictive vocal production. Green frame shows fast trill and blue frame shows slow trills, two distinct phases of the advertisement calls of male *Xenopus laevis*. The long-lasting depolarization of the membrane potential and the repetitive firing during the fast trill is a signature membrane potential activity of the FTNs. *B*: example trace of the membrane potential of the neuron (green plot in *C*) in response to the 10-min bath application of ACh (*left*) and SP (*right*). The parts of the traces with artifact associated with the ligand application and other random noises are removed. *C*: the membrane potentials (average of 30 s) of four FTNs before (pre), peak during (peak), and after (post) the application of ACh (*left*) and SP (*right*). Prior to the experiment, TTX was applied to the whole-brain preparation to block all synaptic transmission mediated by action potentials. Each color indicates data obtained from each neuron ($n = 4$). Based on the response profile, the blue neuron is pFTN-III, and the purple, red, and green neurons are pFTN-IV.

tisement calls (Fig. 6*E*, *middle*). All brains produced fictive calls in response to 5-HT before the atropine/tubocurarine injection (Fig. 6*E*, *left*). One hour after the atropine/tubocurarine injection, when a vehicle (saline, 350 nl each) was injected bilaterally into the PBs of the same brains followed by 5-HT application, fictive advertisement calls were elicited from all the brains (Fig. 6*E*, *right*). The results suggest that the activation of nAChR and/or mAChR of in PB neurons is necessary for vocal production in male *X. laevis*. In contrast, 5-HT application preceded by the bilateral injection of aprepitant did not block fictive vocalizations in any of the brains, although the morphology of 5-HT-induced fictive calls was abnormal (Fig. 6*F*, *middle*). The progressive increase in rate and amplitude of compound action potentials (CAPs), hallmarks of fast trills (Fig. 6, *C* through *F*, *left*, and Fig. 6*G*, *left*), were absent from the fictive calls produced by brains injected with aprepitant; the CAP repetition rates were either set at fast (~60 Hz, $n = 2$) or slow rate (~30 Hz, $n = 1$, Fig. 6*G*), and the CAP amplitude was variable (Fig. 6*G*, *middle*). The application of 5-HT into brains injected with vehicle alone into PB (350 nl 10% DMSO) 1 h after the aprepitant injection produced stereotypical fictive calls with progressive increase in the amplitude and the rate (Fig. 6*G*, *right*). When the cross-correlation coefficients of the CAP amplitude and the CAP instantaneous frequency of fictive advertisement calls were calculated, fictive calls before the aprepitant injection and those elicited with the vehicle injection showed high cross-correlation coefficients (amplitude; 0.901 0.003, 0.786 ± 0.063, instantaneous frequency; 0.859 ± 0.046, 0.776 ± 0.078, mean ± standard deviation for control and vehicle injection), whereas the calls with aprepitant injection showed low cross-correlation coefficients (0.423 ± 0.134, 0.426 ± 0.143 for amplitude and instantaneous fre-

quency). The results show that the aprepitant injection in PB blocked the progressive increase in the CAP rates and amplitude, and the loss of stereotypy of the fictive advertisement calls, suggesting that the SP in PB plays a role in shaping the morphology of fast trills.

Comparison of male and female PB neurons. Male and female *X. laevis* produce sexually distinct vocalizations to coordinate reproduction. A nongravid female clasped by a male produces the release calls that are made of a series of clicks repeated at 6 to 10 Hz, much slower than those of males (Kelley et al. 2017). Local field potential recordings obtained from the PB of female brains during fictive release calls show very little vocal-related activity (A. Yamaguchi and E. Zornik, unpublished observations). However, the application of testosterone to adult females masculinizes their vocalization within 5–13 wk (Potter et al. 2005), and

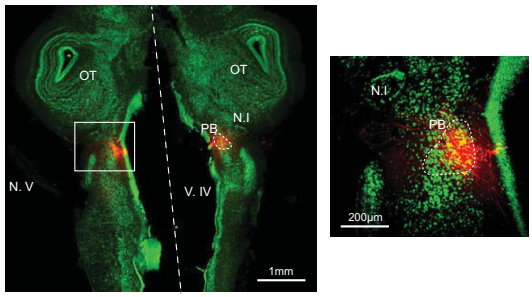

B

Pharmacological agents	Delivery method	n	% brain sang with ligands	% brain sang after washout
ACh	PB injection	8	0	0
SP	PB injection	4	50	100
Saline	PB injection	6	n.a.	100
ACh	bath application	3	0	100
SP	bath application	7	57	100
atr/tbc + 5HT	PB injection	5	0	100
aprepitant + 5HT	PB injection	3	100	100

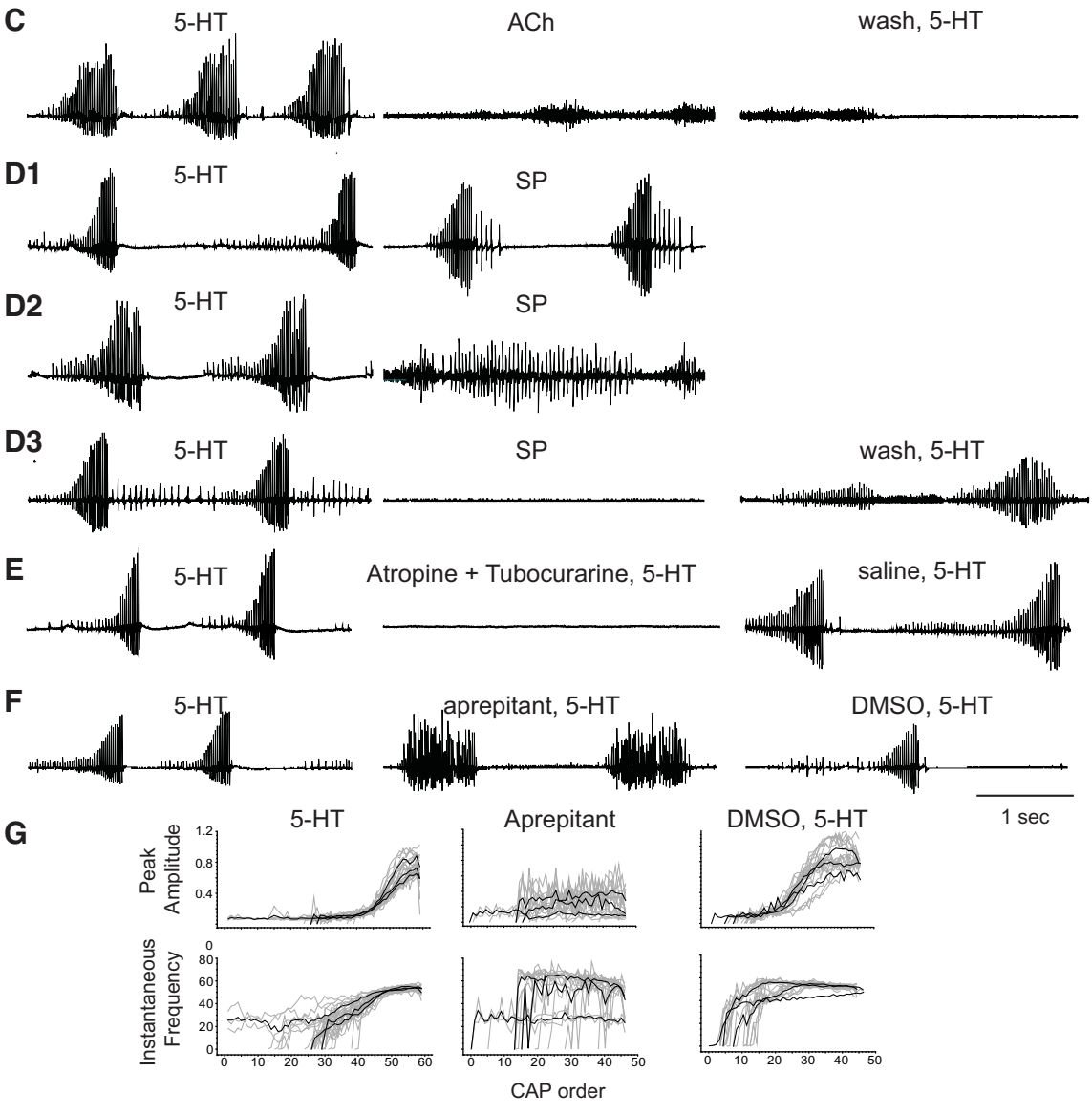

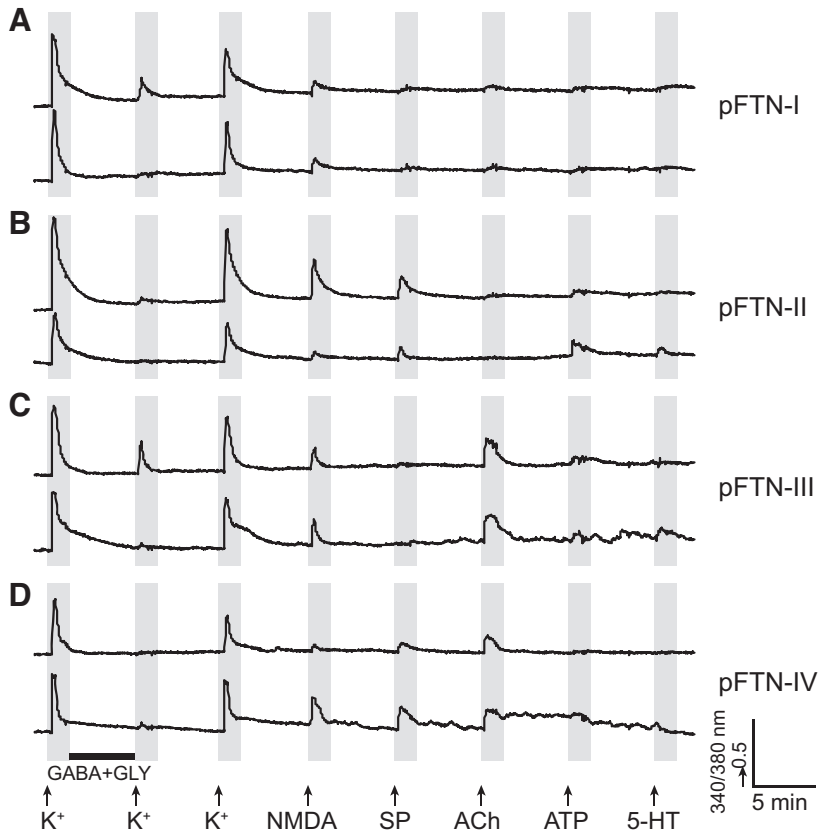

Fig. 7. Example calcium imaging traces of putative fast trill neurons (pFTN) I through IV obtained from female parabrachial nucleus. The *x*- and *y*-axis indicate the time and a relative measurement of cytoplasmic [Ca^{2+}], respectively. Arrows indicate the time at which pharmacological agents were applied, and the black horizontal bar indicates the time during which cells were incubated with GABA and glycine (Gly). NMDA, *N*-methyl-D-aspartate; SP, substance P.

their PBs show strong vocal-related activity during fictive advertisement calls (A. Yamaguchi and E. Zornik, unpublished observations). To determine whether the types and frequency of vocal neurons contained in PB are distinct in the sexes, we compared the types of PB neurons obtained from male and sexually unreceptive female *X. laevis*. Surprisingly, all of the classes and subclasses (listed in Table 2) of PB neurons including all pFTNs identified in males were also found in the dissociated PB cells from sexually unreceptive female *X. laevis* (Fig. 7, *A–D*). Furthermore, the frequency of all the neuron subclasses, including pFTNs, did not differ significantly from between the sexes (Fig. 8). The results suggest that, despite distinct vocalizations produced by the sexes, the PBs of males and females contain neurons with similar molecular profiles at a similar frequency.

Fig. 6. A role of substance P (SP) and acetylcholine (ACh) in the parabrachial (PB) nucleus in the production of fictive vocalizations. *A*: example injection site of agonists and antagonists shown in a horizontal section of the brain of *Xenopus laevis*. The top and the bottom of the images are the rostral and the caudal edge of the tissue, respectively, and the dotted white line indicates the midline. Neurotrace staining is in green, and injection sites are shown in red. A white rectangle area on the left image is enlarged on the right. N.I, nucleus isthmi; N.V., cranial nerve V; OT, optic tectum; V.IV, fourth ventricle. For all the laryngeal nerve recording traces shown in *C* through *F*, the *y*-axis is the same for before (5-HT), during (pharmacological agents), and after (wash, saline, DMSO) the drug injection for each brain, even though the noise is increased in some cases. *B*: summary of the pharmacological experiments. atr/tbc, Cocktail of atropine and tubocurarine; *n*, sample size; % brain sang with ligands, proportion of brains that generated fictive vocalizations (including fast and/or slow trills) in response to the ligand injection or bath application; % brain sang after washout, proportion of the brain that sang in response to the application of 5-HT after the target ligands were washed out for 1–4 h. *C*: laryngeal nerve recordings in response to the bilateral injection of ACh into PB ($n = 6$). *Left*: fictive advertisement calls recorded from the laryngeal nerve in response to the bath application of 5-HT 1 h before ACh injection. *Middle*: laryngeal nerve recordings obtained in response to ACh injected into PBs. *Right*: laryngeal nerve recordings obtained in response to 5-HT application 1 h after ACh was washed out of the bath. *D*: laryngeal nerve recordings in response to the bilateral injection of SP into PBs ($n = 4$). *D1*, *D2*, and *D3* show three different responses observed from four brains injected with SP into PB. *Left*: fictive advertisement calls recorded from the laryngeal nerve in response to the bath application of 5-HT 1 h before SP injection. Right for D1 and D2, middle for D3, laryngeal nerve recordings after SP was injected bilaterally into the PBs. D3. *Right*: fictive advertisement calls recorded from the laryngeal nerve in response to the bath application of 5HT after a 1-h wash of SP injection into PB. *E*: laryngeal nerve recordings in response to the bilateral injection of atropine and tubocurarine followed by 5-HT ($n = 5$). *Left*: fictive advertisement calls recorded from the laryngeal nerve in response to the bath application of 5-HT. *Middle*: laryngeal nerve recordings obtained when atropine and tubocurarine were injected bilaterally into PBs immediately followed by the bath application of 5-HT. *Right*: laryngeal nerve recordings obtained when the vehicle (saline) was bilaterally injected into PB immediately followed by bath application of 5-HT. *F*: laryngeal nerve recordings in response to the bilateral injection of aprepitant immediately followed by 5-HT application ($n = 3$). *Left*: fictive advertisement calls recorded from the laryngeal nerve in response to the bath application of 5-HT. *Middle*: laryngeal nerve recordings obtained when aprepitant was injected bilaterally into PB immediately followed by the bath application of 5-HT. *Right*: laryngeal nerve recordings obtained when the vehicle (10% DMSO in saline) were bilaterally injected into PB followed by bath application of 5-HT. *G*: peak amplitude and instantaneous frequency of the compound action potentials (CAPs) plotted against CAP order for fictive fast trills obtained from brains before, during, and after aprepitant injection into the PBs (data shown in *F*). Gray traces are individual calls ($n = 3$ to 10 calls per animal per treatment), and the black traces are average for each animal for each experimental condition. Note that the CAP amplitude and instantaneous frequency show a progressive increase during fast trills before (5-HT, *left*) and after (DMSO, 5-HT, *right*), but not during bilateral injection of aprepitant into PBs (*middle*).

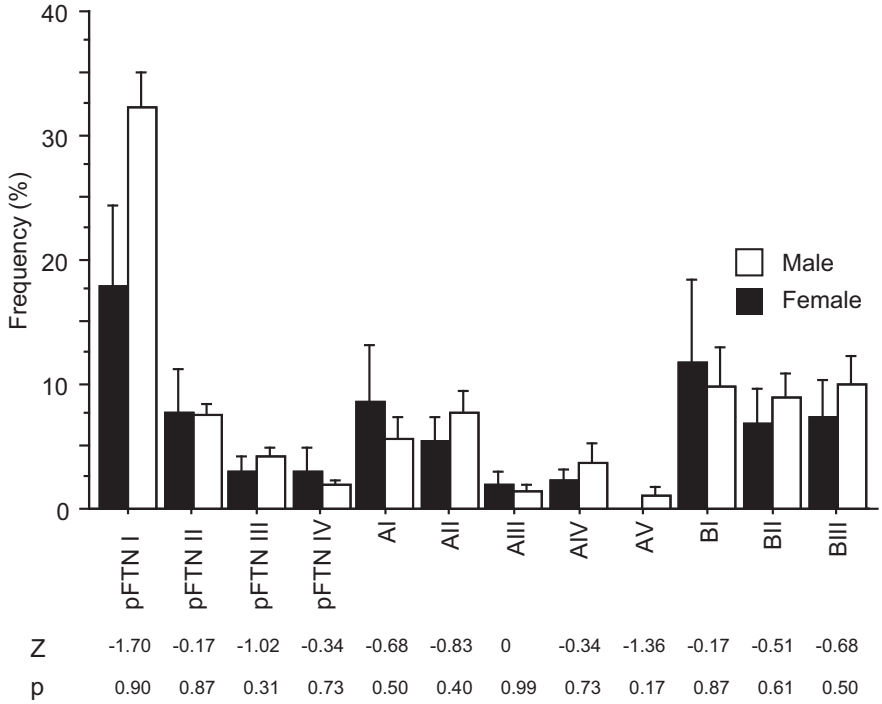

Fig. 8. Frequency histogram of 12 subclasses of parabrachial neurons of adult male ($n = 8$) and female ($n = 4$) *Xenopus laevis*. Each bar indicates the average and standard error. Although males and females produce sexually distinct vocalizations, all 12 subclasses of parabrachial (PB) neurons found in males are also found in females at a similar frequency. Mann–Whitney *U* test, *Z* statistics, and *P* value are shown under the histogram for each cell subclass. Note that none of the comparisons are statistically significant.

DISCUSSION

The results of the present study *1*) revealed previously unknown receptors expressed by the functionally salient vocal neurons, fast trill neurons (FTNs); *2*) discovered the involvement of the newly identified receptors in vocal production; and *3*) identified the similarity in the types and frequency of neurons contained in the vocal nuclei of the sexes despite the sexually distinct vocalizations. The study showcases a powerful methodology for molecular characterization of neurons constituting neural circuitry in all organisms and thus signifies a major step forward in addressing unique questions presented by non-genetic-model organisms.

Using constellation pharmacology, parabrachial (PB) neurons of adult male *X. laevis* were classified. We identified two major classes, A and B, that were further subdivided into a total of 12 subclasses based on their unique response profiles to ligands. In particular, four subclasses of neurons in B class were identified as putative FTNs because of their sensitivity to both NMDA and GABA/glycine, characteristics of FTNs previously identified electrophysiologically (Lawton et al. 2017; Zornik and Yamaguchi 2012). Three of the four putative FTNs (pFTN-II, III, and IV) responded to acetylcholine (ACh) and/or substance P (SP), neurotransmitters whose involvement in the brainstem central vocal pathways were previously unknown. Further electrophysiological experiments obtained from the confirmed FTNs using ex vivo preparation showed that the application of ACh and/or SP to synaptically isolated FTNs indeed depolarize the membrane potentials of FTNs, confirming the prediction derived from the results of constellation pharmacology. Whether the sensitivity to NMDA and GABA is unique to the FTNs within the *X. laevis* PB is currently not known, and thus neurons classified as putative FTNs in this study may have included non-FTNs. Despite this challenge, we were able to identify two additional neuromodulators that modify the membrane potential of the FTNs. These results demonstrate the power of constellation pharmacology together with electrophysiology in identifying key functional molecules expressed by neurons in neural circuitry.

We further tested the roles of the SP and ACh in the vocal productions using ex vivo preparations. Bilateral injection of ACh into PBs (Fig. 6*C*) or its bath application to the isolated brains (Fig. 6*B*) never elicited fictive vocalizations from any of the brains, whereas bilateral injection of SP into PBs (Fig. 6*D*) or its bath application (Fig. 6*B*) elicited fictive vocalizations from about half of the brains. The results suggest that the depolarization of the FTNs by ACh is not sufficient in generating fictive vocalizations, and the potency of SP-mediated FTN activation in eliciting fictive vocalizations is low. In contrast, injection of the antagonists for acetylcholine receptors (AChR) in PBs blocked the 5-HT-induced vocal production (Fig. 6*E*), and the injection of neurokinin-1 receptor (NK-1R) antagonist into PBs resulted in 5-HT-induced vocalizations with abnormal morphology (Fig. 6, *F* and *G*). Thus, the AChR and NK-1R expressed by FTNs play an important role in mediating/modulating vocal production.

One caveat in interpreting the results of the series of pharmacological experiments is as follows. Among dissociated PB neurons, there are subclasses of cells other than pFTNs that respond to ACh and/or SP (Table 2). Thus, the injection of ACh, SP, or their antagonists did not selectively modulate the FTNs, but all PB neurons with the appropriate receptors. Nonetheless, our inability or limited ability to elicit fictive vocalizations with ACh and SP, either by bilateral injection into PBs (Fig. 6, *B* and *C*) or by bath application, is in stark contrast to reliable and repeated activation of fictive vocalizations in response to the bath application of 5-HT, suggesting activation of FTNs by ACh and SP were insufficient in eliciting fictive vocalizations reliably.

One interesting observation we made was that once ACh is injected bilaterally into the PBs, following applications of 5-HT after up to 4 h of wash never elicited fictive vocalizations (Fig. 6, *B* and *C*). This was not the case when ACh was applied

to the bath (Fig. 6*B*); the brains responded to the following 5-HT applications by generating fictive calls after 1 to 2 h of wash. These results may be explained by the internalization or desensitization of cholinergic receptors in PB neurons when they are exposed to a high concentration of the agonists (Giniatullin et al. 2005; Lambert et al. 2018; Wan et al. 2015). The brains that received ACh injections in the PBs may have lost functional cholinergic receptors in PB for a prolonged period of time and thus have become essentially the same as those that received atropine and tubocurarine injections in the PBs and lost their ability to generate fictive vocalizations in response to 5-HT. The experience-dependent change in the availability of cholinergic receptors in PB should be tested in the future to determine the validity of the speculation.

Previously, we demonstrated that fictive vocalizations are elicited by activating 5-HT_{2C} receptors expressed either in the rostral raphe nucleus, the laryngeal motor nucleus, or both (Yu and Yamaguchi 2010). Although the receptors critical for the call initiation may not be expressed by the FTNs, we hypothesized that FTNs may express other types of 5-HT receptors that contribute to the vocal rhythm generations. However, our results showed that the FTNs do not express 5-HT receptors. Together with the results that show that the depolarization of FTNs by SP and ACh is not sufficient to initiate fictive vocalizations reliably, we suggest that FTNs are a part of the vocal rhythm generator that is downstream of the population of 5-HT_{2C}R-positive neurons in the rostral raphe nucleus and/or laryngeal motor nucleus that are responsible for the vocal initiation.

Do NK-1R and AChR also play a role in the activation of the vocal CPGs in other species? Brainstem vocal circuits are known to play a critical role in vocal patterning in a variety of vertebrate species (Hage and Jürgens 2006; Jürgens 2002; Rübsamen and Betz 1986; Schmidt et al. 2012). Although the involvement of AChR in vocal productions has been identified in the forebrains and midbrains of birds, primates, rats, and cats (Brudzynski 2009; Jürgens and Lu 1993; Meng et al. 2017; Silkstone and Brudzynski 2020), roles for AChR and NK-1R in the vertebrate brainstem vocal pathways have not been described. It is possible that NK-1R and AChR may have been repurposed from the neurons contained in the parabrachial nucleus, and/or the brainstem respiratory neural pathways. Both NK-1R and AChR are expressed by neurons in PB of other vertebrate species. For example, muscarinic AChR is found in the PB of cats (Mallios et al. 1995) and rats (Christie and North 1988) and in Kölliker–Fuse nucleus (one of the subdivisions within PB) in goats (Bonis et al. 2010), and NK-1 receptors are found in PB of mice (Boscan et al. 2005). In addition, the activation of NK-1 or ACh receptors of neurons in pre-Bötzinger complex in mice and the paratrigeminal respiratory group of lampreys can enhance respiratory rhythms (Cinelli et al. 2013; Del Negro et al. 2005; Mutolo et al. 2011; Shao et al. 2008). Based on the embryonic origin, vocal CPGs of vertebrates are hypothesized to have evolved from respiratory CPGs located in the brainstem (Bass and Baker 1997). Thus, ACh and NK-1 receptors expressed by FTNs may have derived from the preexisting PB neurons or the neurons in the brainstem respiratory pathways and become adapted to generate vocalizations through evolution.

Male and female *X. laevis* generate sexually distinct vocalizations. Surprisingly, the female PB contained all the classes and subclasses of neurons identified in males at similar frequencies. It is possible that male and female neurons classified as the same pFTN in this study may actually be differentiated by sex-specific receptors and ion channels that were not tested in this study. Single-cell RNA sequencing of male and female pFTNs may allow us to address this question in the future. Nonetheless, there is some evidence suggesting that functional neural circuitry underlying male-specific sexual behavior is present in the female CNS while the mechanisms to activate the circuitry are absent in females. In mice and *Drosophila*, for example, it has been shown that functional neural circuitries for male-specific courtship behavior remain latent in the female brains and can be activated with experimental manipulation, even though females never expressed male-specific courtship behavior in vivo throughout their lives (Clyne and Miesenböck 2008; Kimchi et al. 2007; Rezával et al. 2016). Interestingly, in *X. laevis*, the administration of testosterone to adult females results in vocal masculinization in a relatively short amount of time [5–13 wk (Potter et al. 2005)]. As in mice and *Drosophila*, female *X. laevis* may be equipped with an array of latent neurons including FTNs responsible for male-specific vocal behavior that can be unmasked in the presence of high levels of plasma testosterone.

In this study, we used an integrated approach to identify receptors expressed by neurons critical for the production of vocal behavior. We identified potential receptors expressed by the dissociated neurons using constellation pharmacology, confirmed the functional expression of the receptors by the vocal neurons using whole-cell patch-clamp recordings, and characterized the functional roles played by the receptors expressed by the vocal neurons in generating vocalizations using pharmacology and electrophysiology. This powerful approach is not limited to genetic model organisms but can be applied to any organisms, extending the horizon for research to non-genetic-model organisms that present unique and important questions in the field of neuroscience.

GRANTS

This work was supported by National Science Foundation (NSF) IOS 1557945, 1934386 (A.Y.), NSF IOS 1755423 (E.Z.), NIH NS091977 (E.Z.), and NIH GM48677 (B.O.).

DISCLOSURES

No conflicts of interest, financial or otherwise, are declared by the authors.

AUTHOR CONTRIBUTIONS

R.T.I., S.R., B.M.O., and A.Y. conceived and designed research; R.T.I., S.R., T.S., E.Z., and A.Y. performed experiments; R.T.I., S.R., K.C., T.S., E.Z., and A.Y. analyzed data; R.T.I., S.R., E.Z., B.M.O., and A.Y. interpreted results of experiments; R.T.I., E.Z., and A.Y. prepared figures; R.T.I. and A.Y. drafted manuscript; R.T.I., S.R., K.C., E.Z., and A.Y. edited and revised manuscript; R.T.I., S.R., K.C., T.S., E.Z., B.M.O., and A.Y. approved final version of manuscript.

REFERENCES

Babski H, Jovanic T, Surel C, Yoshikawa S, Zwart MF, Valmier J, Thomas JB, Enriquez J, Carroll P, Garcès A. A GABAergic Maf-expressing interneuron subset regulates the speed of locomotion in Drosophila. *Nat Commun* 10: 4796, 2019. doi:10.1038/s41467-019-12693-6.

Bass AH. Central pattern generator for vocalization: is there a vertebrate morphotype? *Curr Opin Neurobiol* 28: 94–100, 2014. doi:10.1016/j.conb.2014.06.012.

Bass AH, Baker R. Phenotypic specification of hindbrain rhombomeres and the origins of rhythmic circuits in vertebrates. *Brain Behav Evol* 50, *Suppl* 1: 3–16, 1997. doi:10.1159/000113351.

Bonis JM, Neumueller SE, Krause KL, Kiner T, Smith A, Marshall BD, Qian B, Pan LG, Forster HV. A role for the Kolliker-Fuse nucleus in cholinergic modulation of breathing at night during wakefulness and NREM sleep. *J Appl Physiol (1985)* 109: 159–170, 2010. doi:10.1152/japplphysiol.00933.2009.

Boscan P, Dutschmann M, Herbert H, Paton JF. Neurokininergic mechanism within the lateral crescent nucleus of the parabrachial complex participates in the heart-rate response to nociception. *J Neurosci* 25: 1412–1420, 2005. doi:10.1523/JNEUROSCI.4075-04.2005.

Brudzynski SM. Medial cholinoceptive vocaliation strip in the cat and rat brains: initiation of defensive vocalizations. In: *Handbook of Mammalian Vocalization: An Integrative Neuroscience Approach*, edited by Brudzynski SM. London, UK: Academic Press, 2009, p. 265–280.

Caldeira V, Dougherty KJ, Borgius L, Kiehn O. Spinal Hb9:Cre-derived excitatory interneurons contribute to rhythm generation in the mouse. *Sci Rep* 7: 41369, 2017. doi:10.1038/srep41369.

Carmignoto G, Pasti L, Pozzan T. On the role of voltage-dependent calcium channels in calcium signaling of astrocytes in situ. *J Neurosci* 18: 4637–4645, 1998. doi:10.1523/JNEUROSCI.18-12-04637.1998.

Christie MJ, North RA. Agonists at mu-opioid, M2-muscarinic and GABAB-receptors increase the same potassium conductance in rat lateral parabrachial neurones. *Br J Pharmacol* 95: 896–902, 1988. doi:10.1111/j.1476-5381.1988.tb11719.x.

Cinelli E, Robertson B, Mutolo D, Grillner S, Pantaleo T, Bongianni F. Neuronal mechanisms of respiratory pattern generation are evolutionary conserved. *J Neurosci* 33: 9104–9112, 2013. doi:10.1523/JNEUROSCI.0299-13.2013.

Clyne JD, Miesenböck G. Sex-specific control and tuning of the pattern generator for courtship song in Drosophila. *Cell* 133: 354–363, 2008. doi:10.1016/j.cell.2008.01.050.

Curtice KJ, Leavitt LS, Chase K, Raghuraman S, Horvath MP, Olivera BM, Teichert RW. Classifying neuronal subclasses of the cerebellum through constellation pharmacology. *J Neurophysiol* 115: 1031–1042, 2016. doi:10.1152/jn.00894.2015.

Del Negro CA, Morgado-Valle C, Hayes JA, Mackay DD, Pace RW, Crowder EA, Feldman JL. Sodium and calcium current-mediated pacemaker neurons and respiratory rhythm generation. *J Neurosci* 25: 446–453, 2005. doi:10.1523/JNEUROSCI.2237-04.2005.

Doi A, Ramirez JM. Neuromodulation and the orchestration of the respiratory rhythm. *Respir Physiol Neurobiol* 164: 96–104, 2008. doi:10.1016/j.resp.2008.06.007.

Dougherty KJ, Zagoraiou L, Satoh D, Rozani I, Doobar S, Arber S, Jessell TM, Kiehn O. Locomotor rhythm generation linked to the output of spinal shox2 excitatory interneurons. *Neuron* 80: 920–933, 2013. doi:10.1016/j.neuron.2013.08.015.

Eide L, McMurray CT. Culture of adult mouse neurons. *Biotechniques* 38: 99–104, 2005. doi:10.2144/05381RR02.

Funk GD. Neuromodulation: purinergic signaling in respiratory control. *Compr Physiol* 3: 331–363, 2013. doi:10.1002/cphy.c120004.

Gibb S, Strimmer K. MALDIquant: a versatile R package for the analysis of mass spectrometry data. *Bioinformatics* 28: 2270–2271, 2012. doi:10.1093/bioinformatics/bts447.

Giniatullin R, Nistri A, Yakel JL. Desensitization of nicotinic ACh receptors: shaping cholinergic signaling. *Trends Neurosci* 28: 371–378, 2005. doi:10.1016/j.tins.2005.04.009.

Goulding M. Circuits controlling vertebrate locomotion: moving in a new direction. *Nat Rev Neurosci* 10: 507–518, 2009. doi:10.1038/nrn2608.

Grillner S, Jessell TM. Measured motion: searching for simplicity in spinal locomotor networks. *Curr Opin Neurobiol* 19: 572–586, 2009. doi:10.1016/j.conb.2009.10.011.

Hage SR, Jürgens U. On the role of the pontine brainstem in vocal pattern generation: a telemetric single-unit recording study in the squirrel monkey. *J Neurosci* 26: 7105–7115, 2006. doi:10.1523/JNEUROSCI.1024-06.2006.

Haque F, Rancic V, Zhang W, Clugston R, Ballanyi K, Gosgnach S. *WT1*-expressing interneurons regulate left-right alternation during mammalian locomotor activity. *J Neurosci* 38: 5666–5676, 2018. doi:10.1523/JNEUROSCI.0328-18.2018.

Imperial JS, Cabang AB, Song J, Raghuraman S, Gajewiak J, Watkins M, Showers-Corneli P, Fedosov A, Concepcion GP, Terlau H, Teichert RW, Olivera BM. A family of excitatory peptide toxins from venomous crassispirine snails: using Constellation Pharmacology to assess bioactivity. *Toxicon* 89: 45–54, 2014. doi:10.1016/j.toxicon.2014.06.014.

Iredale PA, Dickenson JM. Measurement of intracellular free calcium ion concentration in cell populations using fura-2. *Methods Mol Biol* 41: 203–213, 1995. doi:10.1385/0-89603-298-1:203.

Jürgens U. A study of the central control of vocalization using the squirrel monkey. *Med Eng Phys* 24: 473–477, 2002. doi:10.1016/S1350-4533(02)00051-6.

Jürgens U, Lu CL. Interactions between glutamate, GABA, acetylcholine and histamine in the periaqueductal gray's control of vocalization in the squirrel monkey. *Neurosci Lett* 152: 5–8, 1993. doi:10.1016/0304-3940(93)90469-2.

Kelley DB. Neuroeffectors for vocalization in Xenopus laevis: hormonal regulation of sexual dimorphism. *J Neurobiol* 17: 231–248, 1986. doi:10.1002/neu.480170307.

Kelley DB, Elliott TM, Evans BJ, Hall IC, Leininger EC, Rhodes HJ, Yamaguchi A, Zornik E. Probing forebrain to hindbrain circuit functions in *Xenopus*. *Genesis* 55: e22999, 2017. doi:10.1002/dvg.22999.

Kiehn O. Locomotor circuits in the mammalian spinal cord. *Annu Rev Neurosci* 29: 279–306, 2006. doi:10.1146/annurev.neuro.29.051605.112910.

Kimchi T, Xu J, Dulac C. A functional circuit underlying male sexual behaviour in the female mouse brain. *Nature* 448: 1009–1014, 2007. doi:10.1038/nature06089.

Konishi M. From central pattern generator to sensory template in the evolution of birdsong. *Brain Lang* 115: 18–20, 2010. doi:10.1016/j.bandl.2010.05.001.

Lambert L, Dubayle D, Fafouri A, Herzog E, Csaba Z, Dournaud P, El Mestikawy S, Bernard V. Endocytosis of activated muscarinic m2 receptor (m2R) in live mouse hippocampal neurons occurs via a clathrin-dependent pathway. *Front Cell Neurosci* 12: 450, 2018. doi:10.3389/fncel.2018.00450.

Lawton KJ, Perry WM, Yamaguchi A, Zornik E. Motor neurons tune premotor activity in a vertebrate central pattern generator. *J Neurosci* 37: 3264–3275, 2017. doi:10.1523/JNEUROSCI.2755-16.2017.

Mallios VJ, Lydic R, Baghdoyan HA. Muscarinic receptor subtypes are differentially distributed across brain stem respiratory nuclei. *Am J Physiol* 268: L941–L949, 1995. doi:10.1152/ajplung.1995.268.6.L941.

Marder E, Bucher D. Central pattern generators and the control of rhythmic movements. *Curr Biol* 11: R986–R996, 2001. doi:10.1016/S0960-9822(01)00581-4.

Meng W, Wang S, Yao L, Zhang N, Li D. Muscarinic receptors are responsible for the cholinergic modulation of projection neurons in the song production brain nucleus RA of zebra finches. *Front Cell Neurosci* 11: 51, 2017. doi:10.3389/fncel.2017.00051.

Mutolo D, Cinelli E, Bongianni F, Pantaleo T. Identification of a cholinergic modulatory and rhythmogenic mechanism within the lamprey respiratory network. *J Neurosci* 31: 13323–13332, 2011. doi:10.1523/JNEUROSCI.2764-11.2011.

Potter KA, Bose T, Yamaguchi A. Androgen-induced vocal transformation in adult female African clawed frogs. *J Neurophysiol* 94: 415–428, 2005. doi:10.1152/jn.01279.2004.

Raghuraman S, Garcia AJ, Anderson TM, Twede VD, Curtice KJ, Chase K, Ramirez JM, Olivera BM, Teichert RW. Defining modulatory inputs into CNS neuronal subclasses by functional pharmacological profiling. *Proc Natl Acad Sci USA* 111: 6449–6454, 2014. doi:10.1073/pnas.1404421111.

Ramirez JM, Severs LJ, Ramirez SC, Agosto-Marlin IM. Advances in cellular and integrative control of oxygen homeostasis within the central nervous system. *J Physiol* 596: 3043–3065, 2018. doi:10.1113/JP275890.

Rezával C, Pattnaik S, Pavlou HJ, Nojima T, Brüggemeier B, D'Souza LAD, Dweck HKM, Goodwin SF. Activation of Latent Courtship Circuitry in the Brain of Drosophila Females Induces Male-like Behaviors. *Curr Biol* 26: 2508–2515, 2016. doi:10.1016/j.cub.2016.07.021.

Rhodes HJ, Yu HJ, Yamaguchi A. Xenopus vocalizations are controlled by a sexually differentiated hindbrain central pattern generator. *J Neurosci* 27: 1485–1497, 2007. doi:10.1523/JNEUROSCI.4720-06.2007.

Rübsamen R, Betz M. Control of echolocation pulses by neurons of the nucleus ambiguus in the rufous horseshoe bat, Rhinolophus rouxi. I. Single unit recordings in the ventral motor nucleus of the laryngeal nerves in spontaneously vocalizing bats. *J Comp Physiol A Neuroethol Sens Neural Behav Physiol* 159: 675–687, 1986. doi:10.1007/BF00612040.

Schmidt MF, McLean J, Goller F. Breathing and vocal control: the respiratory system as both a driver and a target of telencephalic vocal motor circuits

in songbirds. *Exp Physiol* 97: 455–461, 2012. doi:10.1113/expphysiol.2011.058669.

Shao XM, Feldman JL. Central cholinergic regulation of respiration: nicotinic receptors. *Acta Pharmacol Sin* 30: 761–770, 2009. doi:10.1038/aps.2009.88.

Shao XM, Tan W, Xiu J, Puskar N, Fonck C, Lester HA, Feldman JL. Alpha4* nicotinic receptors in preBotzinger complex mediate cholinergic/nicotinic modulation of respiratory rhythm. *J Neurosci* 28: 519–528, 2008. doi:10.1523/JNEUROSCI.3666-07.2008.

Silkstone M, Brudzynski SM. Dissimilar interaction between dopaminergic and cholinergic systems in the initiation of emission of 50-kHz and 22-kHz vocalizations. *Pharmacol Biochem Behav* 188: 172815, 2020. doi:10.1016/j.pbb.2019.172815.

Sweeney LB, Kelley DB. Harnessing vocal patterns for social communication. *Curr Opin Neurobiol* 28: 34–41, 2014. doi:10.1016/j.conb.2014.06.006.

Team RC. *R: A Language and Environment for Statistical Computing*. Vienna, Austria: R Foundation for Statistical Computing, 2013.

Teichert RW, Memon T, Aman JW, Olivera BM. Using constellation pharmacology to define comprehensively a somatosensory neuronal subclass. *Proc Natl Acad Sci USA* 111: 2319–2324, 2014. doi:10.1073/pnas.1324019111.

Teichert RW, Raghuraman S, Memon T, Cox JL, Foulkes T, Rivier JE, Olivera BM. Characterization of two neuronal subclasses through constellation pharmacology. *Proc Natl Acad Sci USA* 109: 12758–12763, 2012. doi:10.1073/pnas.1209759109.

Wan M, Zhang W, Tian Y, Xu C, Xu T, Liu J, Zhang R. Unraveling a molecular determinant for clathrin-independent internalization of the M2 muscarinic acetylcholine receptor. *Sci Rep* 5: 11408, 2015. doi:10.1038/srep11408.

Yamaguchi A, Kaczmarek LK, Kelley DB. Functional specialization of male and female vocal motoneurons. *J Neurosci* 23: 11568–11576, 2003. doi:10.1523/JNEUROSCI.23-37-11568.2003.

Yu HJ, Yamaguchi A. Endogenous serotonin acts on 5-HT2C-like receptors in key vocal areas of the brain stem to initiate vocalizations in *Xenopus laevis*. *J Neurophysiol* 103: 648–658, 2010. doi:10.1152/jn.00827.2009.

Zornik E, Yamaguchi A. Coding rate and duration of vocalizations of the frog, Xenopus laevis. *J Neurosci* 32: 12102–12114, 2012. doi:10.1523/JNEUROSCI.2450-12.2012.